Norwegian Meteorological Institute
met.no

met.no report

Report no. 3/2012
Oceanography
ISSN: 1503-8025
Oslo, February 9, 2012

Documentation of simple ocean models for use in ensemble predictions

Part I: Theory

Lars Petter Røed

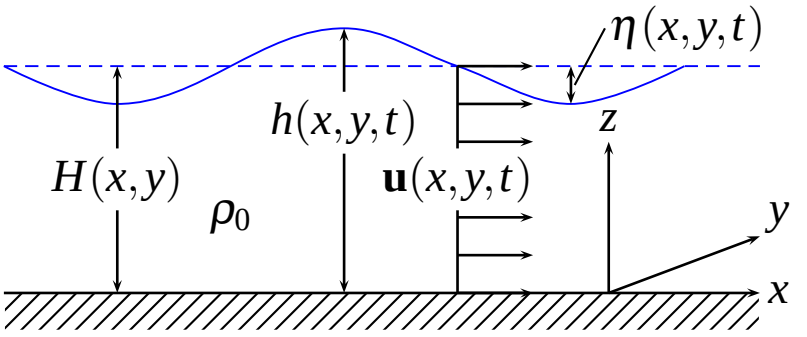

$$\partial_t \eta + \nabla_H \cdot \mathbf{U} = 0,$$
$$\partial_t \mathbf{U} + \nabla_H \cdot \left(\frac{\mathbf{UU}}{H+\eta}\right) + f\mathbf{k}\times\mathbf{U} + \mathbf{P} = \frac{\Delta\boldsymbol{\tau}}{\rho_0} + A\nabla_H^2\mathbf{U},$$

Norwegian Meteorological Institute
met.no

report

Number	Subject	Date	Classification	ISSN
3/2012	Oceanography	February 9, 2012	☒ Open ☐ Restricted ☐ Confidential	1503-8025

Title

Documentation of simple ocean models for use in ensemble predictions

Part I: Theory

Authors

Lars Petter Røed

Client(s)	Client reference
Statoil (Kenneth Eik Johannessen)	Contract No. 4502367955

Abstract

We envisage the use of the Graphical Processor Units rather than conventional Central Processing Units as future tools for numerical ocean weather prediction. As a pilot we first consider implementation of simple ocean models. The models we consider belongs to a class of models referred to as shallow water equations. Here we consider in particular linear and non-linear versions of three models, namely, a one-layer model, a $1\frac{1}{2}$-layer model and a two-layer model. Even today these models are in use, e.g., to predict storm surges. In Part I we present the governing equation of the three models, and develop a set of conditionally stable, finite difference equations based on finite difference approximations of the various terms entering the governing equations of the one-layer model. The finite difference equations for both the linear and the non-linear versions are presented. In Part II we present the numerical solution to several benchmark cases, together with the associated source code written in the FORTRAN language.

Keywords

Physical Oceanography, Numerical Modeling, Shallow water equations, Benchmark solutions

Disiplinary signature	Responsible signature
Lars Anders Breivik, Head Ocean and Ice	Øystein Hov, Head R&D Department

Postal address PO Box 43 Blindern, N-0313 Oslo, Norway
Office Niels Henrik Abels vei 40
Telephone +47 2296 3000
Telefax +47 2296 3050
e-mail: met.inst@met.no **Web:** met.no
Bank account 7695 05 00601
Swift code DNBANOKK

Contents

List of Figures

1 Introduction

We describe three simple ocean models for use in ensemble prediction systems. The first of the three ocean models is a one-layer model featuring a single layer of uniform density as visualized on the front page. The second is a two-layer ocean model featuring two layers of different, but uniform densities. Finally, we consider the so called $1\frac{1}{2}$-layer ocean model. All three models belong to the class of models commonly referred to as shallow water models. The models we consider neglect the effect of changes in the the Earth's rotation with latitude. The Coriolis parameter is thus considered a constant (so called f-plane models).

The one-layer models were commonly used in the 1970s to predict storm surges, that is, the sea surface elevation due to atmospheric forcing (*Martinsen et al.*, 1979, and references therein). The $1\frac{1}{2}$-layer and the two-layer models became quite popular early on to study the upwelling and El Niño phenomena in the ocean (e.g., *Hurlburt et al.*, 1976; *Hurlburt and J. Dana Thompson*, 1976; *Busallacchi and O'Brien*, 1980; *Hurlburt and J. Dana Thompson*, 1980; *Busallacchi and O'Brien*, 1981, and references therein), and later in the 1980s and 1990s to study instabilities, eddies and jet currents in the ocean (e.g., *Luther and O'Brien*, 1985; *Preller*, 1986; *Heburn*, 1988; *McCreary and Kundu*, 1988; *Kindle and Thompson*, 1989; *Heburn and LaViolette*, 1990; *Potemra et al.*, 1991; *Røed*, 1995, 1996, 1997; *Hackett and Røed*, 1998; *Røed*, 1999; *Røed and Shi*, 1999; *Shi and Røed*, 1999, and references therein). The two-layer models were also favored by meteorologists in the 1950s and 1960s to investigate various instability mechanism responsible for the generation of low pressure systems in the atmosphere (*Phillips*, 1957; *Charney and Stern*, 1962).

We note that the $1\frac{1}{2}$-layer model is a variant of the two-layer model in which the thickness of the lower layer is considered to be much larger than the upper layer thickness. This effectively filters out the barotropic mode and leaves a purely baroclinic ocean model.

Why do we consider these simple models? Although they are mostly replaced by much more complex and sophisticated models today that give quite realistic flow patterns, it turns out that their forecast skill is still rather poor. As in meteorology, one way to remedy this situation is to employ data-assimilation. However, in contrast to meteorology, the availability of near real time observations, except for satellite information, is almost nil. Thus we have to look elsewhere. One approach that we consider viable is to make us of ensemble predictions. In an ensemble prediction system (EPS) each member in the ensemble is an equally valid realization of the forecast. Since there are uncertainties in the initial conditions, model parameters, and the forcing, we cannot determine which member that gives the most accurate forecast, but at least we get some information on the uncertainty in the forecast which may be later used to our advantage.

Running todays complex, three-dimensional ocean models in an EPS is a burdensome task even for todays supercomputers. Running more than, say 100 members, is almost unthinkable. Here is where the simpler models comes in. Although the model error increases (simpler models inherently incorporate larger model errors), they run fast and efficient on the computer. Thus we may increase the number of members in our ensemble dramatically. To this end we may in addition investigate the use of Graphical Processing Units (GPUs) rather than the conventional CPUs. GPUs are much faster and require less energy to run. If we are able to produce the ensemble members utilizing the much faster GPUs we may run literally thousands,

and even ten thousands of ensemble members. We may also then explore whether producing a forecast based on thousands of ensemble members using a simple model, that is, introducing a large model error, gives us better forecasts than running one or a few ensembles with a more complex model (smaller model errors).

To obtain some overview of the uncertainty inherent in the simple models, we start the presentation by including how we derive the simple models from the full three-dimensional, Reynolds Averaged Navier Stokes (RANS) equations (Section 2). We also include their associated boundary and initial condition necessary to determine the integration constants. Traditionally we solve the resulting mathematical, continuous differential equations by first replacing them by a set of finite difference equations (FDEs) using finite difference approximations. This is presented in Section 3, and followed by the formulation of the finite difference equations (FDEs) themselves (Section 4). Finally, we end with a summary and some final remarks (Section 5).

We have also implemented the one-layer model on the computer using the FDEs developed here, and run several benchmark cases. In this we make use of the programming language FORTRAN and the computers CPUs. The benchmarks cases, their solutions, and the FORTRAN program are presented in Part II (*Røed*, 2012).

2 Mathematical formulation

2.1 The RANS equations

In the ocean the most prominent dependent variables are the three components u, v, and w of the three-dimensional velocity $\mathbf{v}$, pressure p, density ρ, salinity s, and (potential) temperature θ[1]. To determine these unknowns we need an equal number of equations. These equations are normally referred to as the governing equations since they govern the motion of the two spheres atmosphere and ocean. In a geophysical fluid dynamic (GFD) contest they are also often referred to as the Reynolds Average Navier Stokes (RANS) equation in that they average over the turbulence scale (*Griffies*, 2004).

Of the variables above only the velocity is a vector. The remaining variables, commonly referred to as state variables, are all scalars. Note that salinity and temperature influence the motion via the pressure forcing through the equation of state. The RANS equations are developed based on conservation principles, in our case the conservation of mass, momentum, internal energy and salt content. The RANS equations in their non-Boussinesq form governing oceanic motion are (*Gill*, 1982; *Griffies*, 2004)

$$\begin{aligned}
\partial_t \rho + \nabla\cdot(\rho\mathbf{v}) &= 0, && (1)\\
\partial_t(\rho\mathbf{v}) + \nabla\cdot(\rho\mathbf{v}\mathbf{v}) &= -2\rho\boldsymbol{\Omega}\times\mathbf{v} - \nabla p + \rho\mathbf{g} - \nabla\cdot(\rho\mathscr{F}_M), && (2)\\
\partial_t(\rho\theta) + \nabla\cdot(\rho\theta\mathbf{v}) &= -\nabla\cdot(\rho\mathbf{F}_\theta) + \rho S_\theta, && (3)\\
\partial_t(\rho s) + \nabla\cdot(\rho s\mathbf{v}) &= -\nabla\cdot(\rho\mathbf{F}_s) + \rho S_s, && (4)\\
\rho &= \rho(p,s,\theta). && (5)
\end{aligned}$$

[1] In the following bold upright fonts, e.g., $\mathbf{u}, \mathbf{v}$, are used to denote a vector, while bold special italic fonts, e.g., $\mathscr{U}, \mathscr{V}$, are used to denote tensors

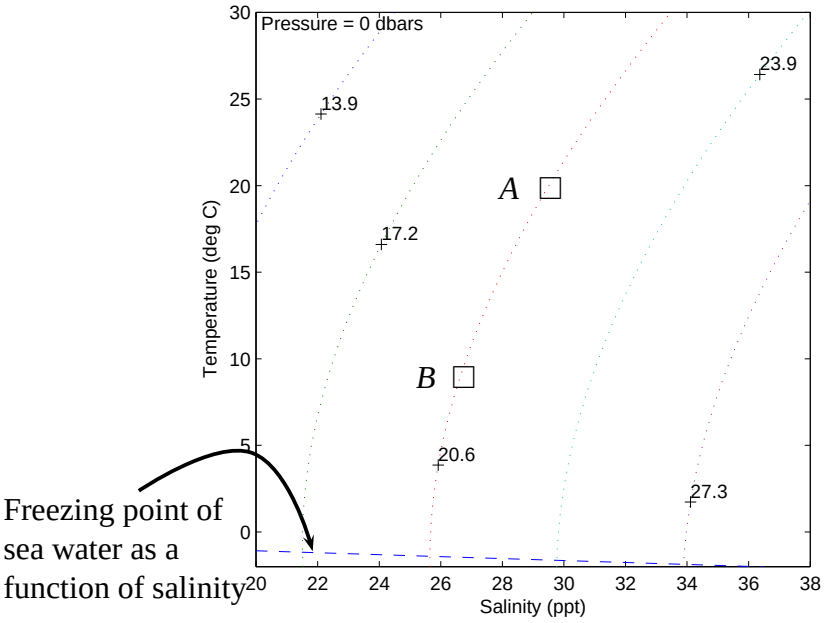

Figure 1: The equation of state for the ocean. Dotted curves show isolines of density as a function of salinity (horizontal axis) and potential temperature (vertical axis) for a fixed reference pressure (here = 0 dbars). Numbers on curves indicate density in σ_t units where $\sigma_t = \rho - 1000$ kg/m^3. Dashed line denotes the freezing point of sea water. Note that for low temperatures (temperatures close to the freezing point of sea water) the density is close to being a function of salinity alone, while the importance of temperature increases with increasing temperature. Due to the non-linear nature of the equation of state for sea water two parcels of water having different temperatures and salinities may still have the same density as for instance the two square points marked A and B along $\sigma_t = 20.6$ kg/m^3.

Here we use ∂_t, ∂_x, ∂_y, and ∂_z to denote partial differential with respect to the respective subscript. Thus $\partial_t \rho$ is the time derivative (or time rate of change) of the density. The tensor $\mathscr{F}_M$ and vectors $\mathbf{F}_s$ and $\mathbf{F}_\theta$ represent fluxes due to turbulent mixing of momentum, salinity and temperature, respectively. $\boldsymbol{\Omega}$ is the Earth's rotation rate, $\mathbf{g}$ is the gravitational acceleration and S_s and S_θ are sources of salinity and heat, if any. Finally, we use ∇ to denote the three-dimensional del-operator defined by

$$\nabla = \mathbf{i}\partial_x + \mathbf{j}\partial_y + \mathbf{k}\partial_z. \tag{6}$$

We note that (1) and (2) constitute mass and momentum conservation, respectively, while conservation of internal energy and salt content gives rise to (3) and (4). Equation (5) is the equation of state which relates density to pressure, salinity and potential temperature.

It should be noted that the equation of state in the ocean is highly non-linear and hence cannot be expressed in a formal, closed mathematical form. We may visualize the equation of

state for the ocean in a so called $\theta - s$ (temperature-salinity) diagram where the salinity s is drawn along the horizontal axis and the (potential) temperature θ is drawn along the vertical axis. Since also pressure enter the equation of state, a $\theta - s$ diagram can only be constructed using a reference pressure. A typical example using the surface pressure as the reference pressure ($p = 0$) is displayed in Figure 1.

2.2 Boundary and initial conditions

To solve (1) - (5) we need to specify conditions at the spatial boundaries of the domain, or the *boundary conditions*, and we need to know the state of the ocean at a particular time, also known as *initial conditions*.

As an example let $\eta = \eta(x,y,t)$ denote the deviation of the sea surface away from its equilibrium level at $z = 0$, and let $H = H(x,y)$ be the equilibrium depth of the ocean[2]. Then the *kinematic* boundary condition at the surface is

$$w = \partial_t \eta + \mathbf{u} \cdot \nabla_H \eta \quad \text{at} \quad z = \eta \tag{7}$$

where $\mathbf{u}, w$ are, respectively, the horizontal and vertical component of the three-dimensional velocity $\mathbf{v}$, and where $\nabla_H = \mathbf{i}\partial_x + \mathbf{j}\partial_y$ is the horizontal component of the three-dimensional del-operator (6). The *dynamic* boundary condition at the surface is

$$p_A = p_O, \quad \text{at} \quad z = \eta \tag{8}$$

where p_A denotes the atmospheric pressure, and p_O the oceanic pressure. The kinematic boundary condition at the bottom of the ocean is similar to (7), that is,

$$w = -\mathbf{u} \cdot \nabla_H H \quad \text{at} \quad z = -H. \tag{9}$$

Note that (7) and (9) assumes that the surface and bottom are are impermeable surfaces, that is, there is no trough-flow across the surface or bottom. We also note that the surface is a Lagrangian surface, that is, it is allowed to change its position as time progresses.

2.3 The hydrostatic and Boussinesq approximations

2.3.1 The hydrostatic approximation

In the ocean the horizontal scales of the dominant motions are mostly large compared to the vertical scale. As a consequence the vertical acceleration, Dw/dt[3], is small in comparison to for instance the gravitational acceleration ρg. Thus in the vertical component of the momentum equation (2), which reads

$$\partial_t(\rho w) + \nabla \cdot (\rho \mathbf{v} w) = -\partial_z p - \rho g - \nabla \cdot (\rho \mathbf{F}_M^V), \tag{10}$$

[2]We assume that the bottom is stationary, that is, does not change in time.

[3]The operator $\frac{D}{dt}$ is the material derivative, or individual derivative, defined by $\frac{D}{dt} = \partial_t + \mathbf{v} \cdot \nabla$.

where $\mathbf{F}_M^V$ is the vertical vector component of the mixing tensor $\mathscr{F}_M$ [4], we may safely neglect all terms except the gravitational acceleration and the pressure forcing. Thus (10) reduces to a balance between the latter two, that is,

$$\partial_z p = -\rho g, \tag{11}$$

which is the *hydrostatic equation*.

When we make use of the hydrostatic equation as our vertical component of the momentum equation, the model is said to be *hydrostatic* and the motion said to satisfy the *hydrostatic approximation*. As alluded to the latter approximation relies on the fact that in most cases the dominant part of the motion, that is, the energetic part is dominated by long waves in shallow water. Hence the horizontal scales of the motion is significantly longer than the vertical scale. Consequently, both the vertical velocity and its acceleration is small compared to the gravitational acceleration. The exceptions are cases that include steep topography and/or strong convection, in which cases one has to revert to non-hydrostatic equations. Assuming that the vertical motion is small compared to the horizontal motion also implies that friction term becomes small as well.

2.3.2 The Boussinesq approximation

Another common approximation employed, and needed to develop the one-layer barotropic model is the *Boussinesq approximation*. The fundamental basis for this approximation is the fact the ocean water is incompressible. This implies that any parcel of fluid conserves its volume, and that this is true even if the parcel is heated. Thus the Boussinesq approximation is only true as long as the change in density for any parcel of fluid is small with respect to the density itself, that is,

$$\frac{1}{\rho}\frac{D\rho}{dt} = \frac{D\ln\rho}{dt} \approx 0, \tag{12}$$

Under the Boussinesq approximation the approximation (12) is taken as an equality. The mass conservation (1) then reduces to

$$\nabla \cdot \mathbf{v} = 0. \tag{13}$$

In practice it turns out that the Boussinesq approximation implies that the density may be treated as a constant except when it appears together with the gravitational acceleration. Thus in the two horizontal components of the momentum equation, and in the conservation equation for internal energy and salt content, the density may be replaced by a reference density, say ρ_0, while in the vertical momentum equation it must be treated as a dependent variable.

[4] We note that in a Cartesian coordinate system fixed to the Earth's surface the vertical component of the Coriolis force is small compared to the gravitational pull. The former is therefore dropped in (10).

2.4 The Boussinesq ocean model

It is quite common to combine the Boussinesq and the hydrostatic equations. Under these circumstances the governing equations reduce to

$$\begin{aligned}
\nabla_H \cdot \mathbf{u} + \partial_z w &= 0, && (14)\\
\partial_t \mathbf{u} + \nabla_H \cdot (\mathbf{uu}) + \partial_z (w\mathbf{u}) + f\mathbf{k}\times\mathbf{u} &= -\rho_0^{-1}\nabla_H p + \rho_0^{-1}\partial_z \boldsymbol{\tau} - \nabla_H \cdot (\mathscr{F}_M^H), && (15)\\
\partial_z p &= -\rho g, && (16)\\
\partial_t \theta + \nabla_H \cdot (\theta\mathbf{u}) + \partial_z (\theta w) &= -\partial_z F_\theta^V - \nabla_H \cdot \mathbf{F}_\theta^H + S_\theta, && (17)\\
\partial_t s + \nabla_H \cdot (s\mathbf{u}) + \partial_z (sw) &= -\partial_z F_s^V - \nabla_H \cdot \mathbf{F}_s^H + S_s, && (18)\\
\rho &= \rho(p,\theta,s). && (19)
\end{aligned}$$

Equations (14) - (19) then constitute a set of seven equations to solve for the seven unknowns u, v, w, p, ρ, θ, and s. We note that when applying the hydrostatic and Boussinesq approximation the vertical velocity component and the density are reduced to *diagnostic variables* just as pressure. This is in contrast to the horizontal velocity components $\mathbf{u}$, potential temperature θ, and s, which are *prognostic variables* in the sense that they are governed by *prognostic equations*, that is, equations containing a time rate of change term of the variable in question.

We note that the surface value of the shear stress, say $\boldsymbol{\tau}_s$, represents the traction of the wind on the ocean surface. Hence it is the energy input via the work $\mathbf{u}_s \cdot \boldsymbol{\tau}_s$ done at the surface, $\mathbf{u}_s$ being the surface current. In the benchmark cases presented in Part II *Røed* (2012) we specify $\boldsymbol{\tau}_s$. It should be emphasized though that the wind stress represents the momentum flux from the atmosphere to the ocean, and hence it is more often than not computed as a function of the wind. In its simplest form the wind stress may be parameterized as (e.g., *Martinsen et al.*, 1979)

$$\boldsymbol{\tau}_s = \rho_a C_D \mathbf{W}_g |\mathbf{W}_g|, \tag{20}$$

where ρ_a is the air density commonly set to $\rho_a = 1.3$ kg/m^3 , C_D is a drag coefficient commonly given the value $C_D = 3.0\cdot 10^{-3}$, and $\mathbf{W}_g$ is the geostrophic wind. A more sophisticated parameterization, and commonly used in more complex models, is that given in *Engedahl* (1995b),

$$\boldsymbol{\tau}_s = \rho_a C_D |\mathbf{W}| \mathbf{W}, \tag{21}$$

where $\mathbf{W}$ is the wind velocity at 10 m height, and where the drag coefficient depends on the wind speed, that is,

$$C_D = \begin{cases} 0.0012 & \text{if } |\mathbf{W}| < 11m/s, \\ (0.49 + 0.065)|\mathbf{W}| & \text{if } |\mathbf{W}| \geq 11m/s. \end{cases} \tag{22}$$

Similarly we note that the stress on the bottom, say $\boldsymbol{\tau}_b$, represents the loss of energy through the work done by friction at the solid bottom. It therefore gives an energy loss on all wave lengths. In its simplest form this term is parameterized as Rayleigh friction, that is,

$$\boldsymbol{\tau}_b = \gamma \mathbf{u}_b, \tag{23}$$

where $\mathbf{u}_b$ is either the velocity at or near the bottom, or simply the mean depth current.

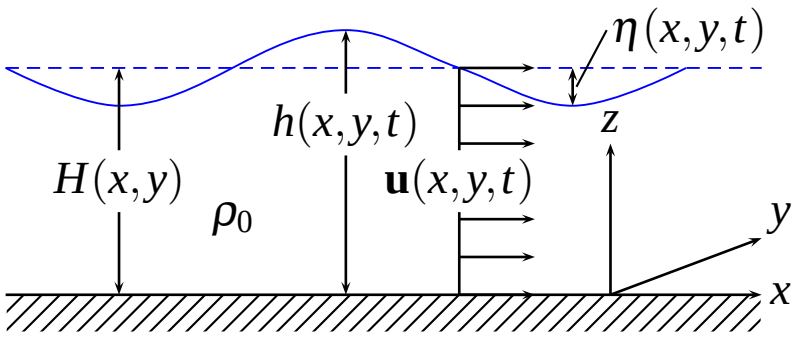

Figure 2: Sketch of a one layer, barotropic model conveniently showing some of the notation. Note that $h = h(x,y,t) = \eta(x,y,t) + H(x,y)$.

Finally we note that (14) - (19) are the common basis for most of the complex, three dimensional, barotropic-baroclinic ocean models used today, e.g., ROMS (http://www.myroms.org/), NEMO (http://www.nemo-ocean.eu/), HYCOM (http://hycom.org/) and POM (http://www.aos.princeton.edu/WW

2.5 The one-layer model

If we in addition to the above Boussinesq and hydrostatic approximation also assume that the density is uniform in time and space, i.e., $\rho = \rho_0$ where ρ_0 is a constant, the governing equations reduces to

$$\nabla_H \cdot \mathbf{u} + \partial_z w = 0 \tag{24}$$

$$\partial_t \mathbf{u} + \nabla_H \cdot (\mathbf{u}\mathbf{u}) + \partial_z (w\mathbf{u}) = -f\mathbf{k}\times\mathbf{u} - \rho_0^{-1}\nabla_H p + \rho_0^{-1}\partial_z \boldsymbol{\tau} - \nabla_H \cdot \mathscr{F}_M^H, \tag{25}$$

$$\partial_z p = -\rho_0 g. \tag{26}$$

Note that when the density is constant the conservation equations for internal energy (17), the salinity equation (18) and the equation of state (19) are all obsolete. Figure 2 provides a sketch of such a model and conveniently shows some of the notation used in below.

We note the assumption of a uniform density allow us to integrate (26) from any arbitrary depth z to the surface $z = \eta(x,y,t)$, that is,

$$p = p_s + g\rho_0(\eta - z) \tag{27}$$

where p_s is the pressure at the sea surface and η is the deviation of the sea surface from its equilibrium level $z = 0$ as sketched in Figure 2. Thus the pressure forcing in (28) becomes

$$\nabla_H p = \nabla_H p_s + \rho_0 g \nabla_H \eta. \tag{28}$$

Substituting (28) into (25) and integrating (24) and (25) from the bottom $z = -H(x,y)$ to the top $z = \eta(x,y,t)$ we get,

$$\partial_t \eta + \nabla_H \cdot \mathbf{U} = 0, \tag{29}$$

$$\partial_t \mathbf{U} + \nabla_H \cdot \left(\frac{\mathbf{U}\mathbf{U}}{H+\eta}\right) + f\mathbf{k}\times\mathbf{U} + \mathbf{P} = \frac{\Delta\boldsymbol{\tau}}{\rho_0} + A\nabla_H^2 \mathbf{U}, \tag{30}$$

where

$$\mathbf{P} = gH\nabla_H \eta + \frac{1}{2} g \nabla_H \eta^2 + \frac{H+\eta}{\rho_0} \nabla_H p_s. \tag{31}$$

To derive (29) and (30) we have used the kinematic boundary conditions (7) and (9) and the dynamic boundary condition $p = p_s$ at $z = \eta$. Here $\mathbf{U} = \int_{-H}^{\eta} \mathbf{u} dz$ is the volume flux or volume transport of fluid through a fluid column of depth $h = H + \eta$, $\Delta\boldsymbol{\tau} = \boldsymbol{\tau}_s - \boldsymbol{\tau}_b$ where $\boldsymbol{\tau}_s$ and $\boldsymbol{\tau}_b$ are, respectively, the turbulent vertical momentum fluxes at the top and bottom of the fluid column, commonly called the wind stress and bottom stress, respectively. The last term in (30) is an explicit parameterization of the last term on the right-hand side of (25) as a diffusive process, that is, $\mathscr{F}_M^H = -A\nabla_H \mathbf{U}$ where A is a constant referred to as the eddy viscosity coefficient. We observe that this term is necessary to avoid non-linear, numerical instabilities to appear (*Haltiner and Williams*, 1980). Finally we note that we have absorbed the term arising from the approximation

$$\int_{-H}^{\eta} \nabla_H \cdot (\mathbf{uu}) dz \approx \nabla_H \cdot (\frac{\mathbf{UU}}{h}) \tag{32}$$

into the last term on the right-hand side of (30). We commonly refer to (30) and (29) as the *barotropic non-linear, shallow water equations*. Written in this form they are said to be written in flux form.

These equation may be linearized assuming that the deviations away from a mean is small, in which case (29) and (30) reduce to

$$\partial_t \eta + \nabla_H \cdot \mathbf{U} = 0, \tag{33}$$

$$\partial_t \mathbf{U} + f\mathbf{k} \times \mathbf{U} + gH\nabla_H \eta + \frac{H}{\rho_0} \nabla_H p_s = \frac{\boldsymbol{\tau}_s - \boldsymbol{\tau}_b}{\rho_0}, \tag{34}$$

which are the barotropic, linear, shallow water equations. Note that we have dropped the explicit eddy viscosity term since there is no energy cascade towards higher wave numbers in this case, and hence no non-linear numerical instabilities to avoid. Furthermore, we are now using the volume transports as our dependent variables, and thus the bottom stress parameterization (23) is replaced by

$$\boldsymbol{\tau}_b = \rho_0 \frac{R}{H} \mathbf{U}, \tag{35}$$

where R is a friction coefficient commonly set to $R = 2.4 \cdot 10^{-3}$ m/s (*Martinsen et al.*, 1979).

2.6 The two-layer model

Commonly the ocean is stratified in the vertical. Stratification has the effect that surfaces of constant pressure and surfaces of constant densities do not necessarily coincide. If this is the case, which is more often the case than not, the model is called baroclinic. The assumption of a constant density is therefore in general not a very realistic assumption. However, when dealing with, e.g., storm surge problems[5] and tidal elevations it turns out that the stratification

[5] Storm surges are water level changes due to atmospheric forcing, mainly mean sea level pressure and wind traction

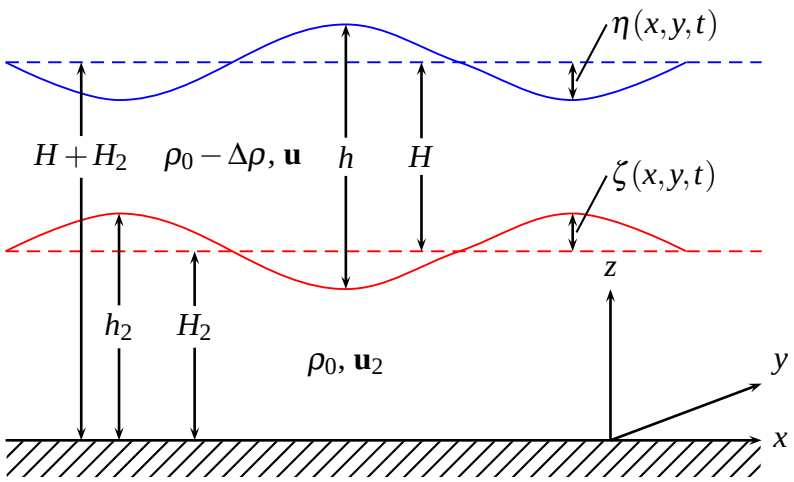

Figure 3: Sketch of a two-layer ocean model of thicknesses $h = h(x,y,t)$ and $h_2 = h_2(x,y,t)$ and densities $\rho - \Delta\rho$ and ρ_0, respectively. We note that $h = H + \eta$ while $h_2 = H_2 + \zeta$.

has a minor effect, and thus may safely be neglected (*Røed*, 1979). For most other oceanic problems the baroclinicity is, however, of zero order importance.

The simplest baroclinic ocean model is the two-layer model as sketched in Figure 3. The model consists of two layers of different yet constant densities. To be statically stable the lower layer is heavier than the upper layer, here by an amount $\Delta\rho$. The density in the upper layer is hence $\rho = \rho_0 - \Delta\rho$ and its thickness is $h = h(x,y,t)$, while the lower layer has density ρ_0 and thickness $h_2 = h_2(x,y,t)$. In equilibrium their thickness are respectively H and $H_2 = H_2(x,y)$. We note that all the layer thicknesses varies in time and space, except the upper layer equilibrium thickness that is constant.

We also note that the motion is governed by the governing equations of the Boussinesq ocean model. Moreover since the density is constant within each layer, the motion within each layer is in fact governed by (24) - (26). As for the one-layer barotropic model we may hence integrate (26) vertically within each layer to derive the pressure at an arbitrary depth z within the layer. Thus integrating the hydrostatic equation (11) from an arbitrary depth in the upper layer to the top, and letting the surface (or atmospheric pressure) $p_s = 0$, we get

$$p = (\rho_0 - \Delta\rho)g(\eta - z)\forall \quad \eta < z < -H + \zeta, \tag{36}$$

where p is the pressure in the upper layer. Likewise, integrating (26) from an arbitrary depth in the lower layer to the interface, we get

$$p_2 = (\rho_0 - \Delta\rho)gh + \rho_2 g(-H + \zeta - z)\forall \quad -H + \zeta < z < -H - H_2, \tag{37}$$

where p_2 is the pressure in the lower layer. To arrive at (36) and (37) we have used (8) and $p = p_s = 0$ at $z = \eta$. In addition we have used the dynamic boundary condition $p = p_2$ at $z = -H + \zeta$ where ζ is the deviation of the interface away from its equilibrium position at $z = -H$ (Figure 3), which is the dynamic boundary condition. For later convenience we note

that the deviations η and ζ may also be written as functions of the layer thicknesses, that is,

$$\eta = (h-H)+(h_2-H_2) = h+h_2-H-H_2 \quad (38)$$
$$\zeta = h_2-H_2, \quad (39)$$

where h is the thickness of the upper layer and h_2 is the thickness of the lower layer.

Integrating the continuity equation (24) first from the interface $z=-H+\zeta$ to the surface $z=\eta$, and then from the bottom $z=-H-H_2$ to the interface, and making use of the kinematic boundary conditions at the top, at the interface and the bottom, we get

$$\partial_t h + \nabla_H \cdot \mathbf{U} = 0, \quad (40)$$
$$\partial_t h_2 + \nabla_H \cdot \mathbf{U}_2 = 0, \quad (41)$$

where $\mathbf{U}$ and $\mathbf{U}_2$ are the volume transports in the upper and lower layer, respectively. Thus the continuity equation simply says that the local time rate of change of the respective thicknesses are proportional to the divergence of the transport in each layer. We note that the thickness is the volume per areal unit. Thus this results is expected since under the Boussinesq approximation the continuity equation implies conservation of volume. Adding (40) and (41) we get

$$\partial_t(H+H_2+\eta)+\nabla_H\cdot(\mathbf{U}+\mathbf{U}_2)=0. \quad (42)$$

We note from (42) that if the transports in the upper and lower layer compensate each other exactly, that is, if $\mathbf{U}=-\mathbf{U}_2$, then the time rate of change of the total thickness of a fluid column is zero. Thus if the thickness of the lower layer increases then this increase may be compensated either by 1) a similar increase in the total water depth $H+H_2+\eta$ (the sea surface experiences a similar increase), or 2) by a similar decrease in the upper layer thickness without any change in the sea surface elevation (Figure 4). The first one is called a *barotropic response*, and corresponds to the response as if the model was a one-layer model of constant density throughout the water column. The second one is called a *baroclinic response* since it takes into account that the two-layer model is baroclinic. In most cases the response is a combination of the two, and that such a model therefore is referred to as a barotropic-baroclinic ocean model. We note that the pure baroclinic response requires that $\mathbf{U}=-\mathbf{U}_2$ is satisfied for all times. This is the same as requiring

$$h\mathbf{u} = -h_2\mathbf{u}_2. \quad (43)$$

We now integrate the momentum equation vertically over each layer separately. We also assume that the currents are almost uniform with depth within each layer, and what is left may be accounted for in the eddy viscosity term. We then get

$$\partial_t\mathbf{U}+\nabla_H\cdot\left(\frac{\mathbf{U}\mathbf{U}}{h}\right)+f\mathbf{k}\times\mathbf{U}+\mathbf{J} = \rho_0^{-1}\Delta\boldsymbol{\tau}+A\nabla_H^2\mathbf{U}, \quad (44)$$
$$\partial_t\mathbf{U}_2+\nabla_H\cdot\left(\frac{\mathbf{U}_2\mathbf{U}_2}{h_2}\right)+f\mathbf{k}\times\mathbf{U}_2+\mathbf{J}_2 = \rho_0^{-1}\Delta\boldsymbol{\tau}_2+A\nabla_H^2\mathbf{U}_2. \quad (45)$$

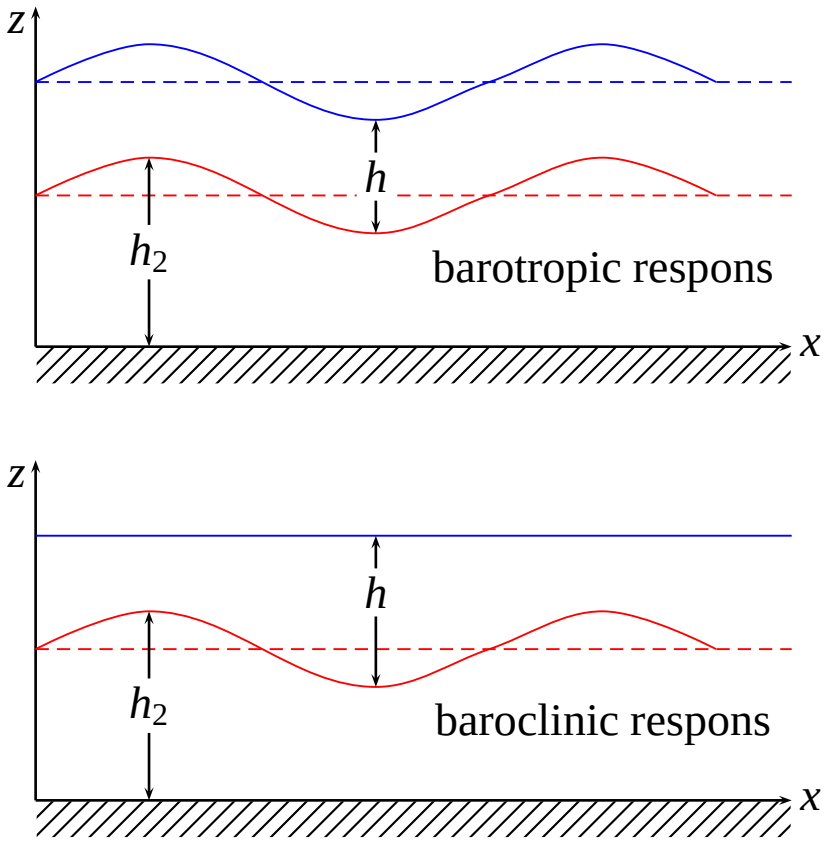

Figure 4: As Figure 3. The figure illustrates the difference between a purely barotropic response (upper panel) and a purely baroclinic response (lower panel) for a two-layer model.

Here

$$\mathbf{J} = gh\nabla_H[(1-\varepsilon)(h+h_2-H-H_2)] = gh(1-\varepsilon)\nabla_H\eta, \tag{46}$$

and

$$\mathbf{J}_2 = gh_2\nabla_H[(1-\varepsilon)h+h_2-H-H_2] = gh_2(1-\varepsilon)\nabla_H\eta + gh_2\nabla_H\zeta, \tag{47}$$

are the pressure forces in the upper and lower layer respectively. The variable $\varepsilon = \Delta\rho/\rho_0$ is referred to as the reduced density. Furthermore,

$$\Delta\boldsymbol{\tau} = \boldsymbol{\tau}_s - \boldsymbol{\tau}_I, \quad \Delta\boldsymbol{\tau}_2 = \boldsymbol{\tau}_I - \boldsymbol{\tau}_b, \tag{48}$$

where $\boldsymbol{\tau}_I$ is the turbulent shear stress at the interface. $\Delta\boldsymbol{\tau}$ is therefore the difference between the shear stress at the surface and the interface, while $\Delta\boldsymbol{\tau}_2$ is the difference between the shear stresses at the interface and the bottom. To arrive at (46) we have also made use of (36) and (37) and the dynamic condition that the shear stresses must be continuous at the interface.

Thus for each layer the governing equations are,

$$\partial_t h + \nabla_H \cdot \mathbf{U} = 0, \tag{49}$$

$$\partial_t \mathbf{U} + \nabla_H \cdot \left(\frac{\mathbf{U}\mathbf{U}}{h}\right) + f\mathbf{k}\times\mathbf{U} + \mathbf{J} = \rho_0^{-1}\Delta\boldsymbol{\tau} + A\nabla_H^2\mathbf{U}, \tag{50}$$

and

$$\partial_t h_2 + \nabla_H \cdot \mathbf{U}_2 = 0, \tag{51}$$

$$\partial_t \mathbf{U}_2 + \nabla_H \cdot \left(\frac{\mathbf{U}_2\mathbf{U}_2}{h_2}\right) + f\mathbf{k}\times\mathbf{U}_2 + \mathbf{J}_2 = \rho_0^{-1}\Delta\boldsymbol{\tau}_2 + A\nabla_H^2\mathbf{U}_2, \tag{52}$$

respectively, that is, six equations for the six unknowns U, U_2, V, V_2, h and h_2.

We note the two sets (49) and (50) and (51) and (52) are formally similar to the one-layer set (30) and (29). Thus both belong to the class of equations called shallow water equations. The two-layer model is hence made up of a stack of two one-layer, shallow water models that exchange momentum through the pressure term and the interface stress term.

We note that if $\varepsilon = 0$, that is, if $\rho = \rho_0$ then the densities are equal in the two layers, and the two-layer model reduces to a one-layer model. Moreover, since ε in the ocean is a very small number, terms of order $\mathcal{O}(\varepsilon^2)$, may safely be neglected compared to terms of order $\mathcal{O}(\varepsilon)$. Note that we have retained terms of order $\mathcal{O}(\varepsilon)$ although they are small compared to terms of $\mathcal{O}(1)$. The rationale is that if $h \ll h_2$ then terms of order $\mathcal{O}(1)$ in the pressure forcing cancel each other.

As for the one-layer model these equations may be linearized. Thus their linear versions read

$$\partial_t h = -\nabla_H \cdot \mathbf{U}, \tag{53}$$

$$\partial_t \mathbf{U} = -f\mathbf{k}\times\mathbf{U} - g'H\nabla_H\eta + \rho_0^{-1}\Delta\boldsymbol{\tau} \tag{54}$$

$$\partial_t h_2 = -\nabla_H \cdot \mathbf{U}_2, \tag{55}$$

$$\partial_t \mathbf{U}_2 = -f\mathbf{k}\times\mathbf{U}_2 - g'H_2\nabla_H(\eta+\zeta) + \rho_0^{-1}\Delta\boldsymbol{\tau}_2, \tag{56}$$

respectively, where $g' = \varepsilon g$ is the reduced gravity.

2.7 The $1\frac{1}{2}$-layer model

We now assume that the lower layer depth is large compared to the upper layer equilibrium thickness everywhere and for all times. Mathematically this implies that $h \ll h_2$ for all times everywhere. Under these circumstances it impossible to maintain a barotropic response. Thus the response turns into a pure baroclinic one. According to (43) the layer transports must then be equal of sign and of opposite direction. Thus $|h\mathbf{u}| = |h_2\mathbf{u}_2|$. Since $h \ll h_2$ this implies that $|\mathbf{u}_2| \ll |\mathbf{u}|$. In turn follows that $|\mathbf{u}_2| \to 0$ when $(h_2/h) \to \infty$. From (44) we observe that we achieve the latter by letting the pressure force in the lower layer be zero. From (47) we then get

$$\mathbf{J}_2 \approx 0 \quad \Rightarrow \quad \nabla_H(h_2 - H - H_2) \approx -(1-\varepsilon)\nabla_H h_1. \tag{57}$$

By substituting this into (46) we get

$$\mathbf{J} \approx \varepsilon g h \nabla_H h = \frac{1}{2} g' \nabla_H h^2, \tag{58}$$

when neglecting terms of order $\mathscr{O}(\varepsilon^2)$. We notice that it in this case it is paramount to keep terms of order $\mathscr{O}(\varepsilon)$ in (46) and (47) since now we assume $h \ll h_2$. In summary we may thus neglect the motion in the lower layer, and hence (52) and (51) becomes obsolete. For the upper layer governing equations we get

$$\begin{aligned} \partial_t h &= -\nabla_H \cdot \mathbf{U}, & (59)\\ \partial_t \mathbf{U} &= -\nabla_H \cdot \left(\frac{\mathbf{U}\mathbf{U}}{h}\right) - f\mathbf{k}\times\mathbf{U} - \frac{1}{2} g' \nabla_H h^2 + \rho_0^{-1}\Delta\boldsymbol{\tau} + A\nabla_H^2 \mathbf{U}. & (60) \end{aligned}$$

We observe that (60) and (59) are quite similar to (30) and (29), and obviously belong to the shallow water equation class. There are differences though. Most prominent, is the difference in the pressure term. Variations in the bottom topography (spatial variations in H_2) is now neglected, and the ordinary gravitational acceleration is replaced by the reduced gravity. As shown by *Cushman-Roisin and O'Brien* (1983) it is possible though to retain the first order effect of a spatially varying bottom topography. To first order in the parameter $\frac{H}{H_2}$ they found that the reduced gravity g' is replaced by

$$g^* = g'\left(1 + \frac{H}{H_2}\right)^{-1}. \tag{61}$$

Thus when $H/H_2 \to 0$ we observe that $g^* \to g'$. Hence (60) and (59) are recovered. Another and less prominent difference is that the bottom stress is replaced by the interface stress.

Similar to (30) and (29) also (60) and (59) may be linearized in which case we get

$$\begin{aligned} \partial_t h + \nabla_H \cdot \mathbf{U} &= 0, & (62)\\ \partial_t \mathbf{U} + f\mathbf{k}\times\mathbf{U} &= -g' H \nabla_H h + \rho_0^{-1}\Delta\boldsymbol{\tau}. & (63) \end{aligned}$$

Again we have dropped the eddy viscosity term since it is no longer needed.

3 Finite difference formulation of the one-layer model

We start by rewriting the governing equations (30) and (29) of the one-layer model in scalar form. Hence we get

$$\begin{aligned} \partial_t U - fV &= -\partial_x\left(\frac{U^2}{H+\eta}\right) - \partial_y\left(\frac{UV}{H+\eta}\right) - gH\partial_x\eta - \frac{1}{2}g\partial_x\eta^2 + X + A\nabla_H^2 U, & (64)\\ \partial_t V + fU &= -\partial_x\left(\frac{UV}{H+\eta}\right) - \partial_y\left(\frac{V^2}{H+\eta}\right) - gH\partial_y\eta - \frac{1}{2}g\partial_y\eta^2 + Y + A\nabla_H V, & (65)\\ \partial_t \eta &= -\partial_x U - \partial_y V, & (66) \end{aligned}$$

where we have set $p_s = 0$. We also note that $H = H(x,y)$ is the equilibrium depth. Furthermore we have replaced the stress terms by X and Y, respectively. Thus

$$X = \frac{\tau_s^x}{\rho_0} - \frac{R}{H}U, \tag{67}$$

and

$$Y = \frac{\tau_s^y}{\rho_0} - \frac{R}{H}V. \tag{68}$$

In linear form these equations reduces to

$$\begin{aligned} \partial_t U - fV &= -gH\partial_x \eta + X, & (69)\\ \partial_t V - fU &= -gH\partial_y \eta - Y, & (70)\\ \partial_t \eta &= -\partial_x U - \partial_y V. & (71) \end{aligned}$$

Note that in both the non-linear and linear cases the effect of a spatially varying bottom topography is retained since $H = H(x,y)$. Thus it works through the pressure term and in the non-linear advection terms. Furthermore note that in the linear version we replace h with η as variable.

To obtain consistent, centered in time and centered in space, second order accurate finite difference (FD) formulations for each term in (64) - (66), and in (69) - (71), we make use of Taylor series expansions. Thus at each point in our numerical grid we replace the continuous derivatives with a finite difference approximation by truncating Taylor series. The grid we employ is displayed in Figure 5, and corresponds to lattice C of *Mesinger and Arakawa* (1976). The rationale is that the inherent staggering avoids specifying more boundary conditions than necessary to determine the integration constants. The grid is oriented so that the x-axis in a Cartesian coordinate system points in the east-west direction (positive eastward) and the y-axis in the north-south direction (positive northward).

We note that the U-, V-, and h-grids are staggered, so that compared to the h-grid the U-grid is staggered one half grid length along the x-axis, while the V-grid is staggered one half grid length along the y-axis. As indicated in Figure 5 we count cells rather than points. This avoids the use of the cumbersome half indexes. There is a total of $J+1$ times $K+1$ cells counted using the dummy indexes j,k along the x- and y-axes, respectively. To keep track of the geographic location of the various grid points we let origo be located half a grid length away from the h-point in grid cell number (1,1) in both horizontal directions. Thus, as is common when employing the staggered C-grid, the x-axis goes through V-points, while the y-axis goes through U-points. We may then let any north-south closed boundaries go through U-points, and east-west closed boundaries go through V-points as sketched in Figure 6. We return to this point when discussing the boundary condition in Section 4.4.

Accordingly we use the notation

$$\begin{aligned} h_{jk}^n &= h(x_j - \frac{1}{2}\Delta y, y_k - \frac{1}{2}\Delta y, t^n), & (72)\\ U_{jk}^n &= U(x_j, y_k - \frac{1}{2}\Delta y, t^n), & (73)\\ V_{jk}^n &= V(x_j - \frac{1}{2}\Delta x, y_k, t^n). & (74) \end{aligned}$$

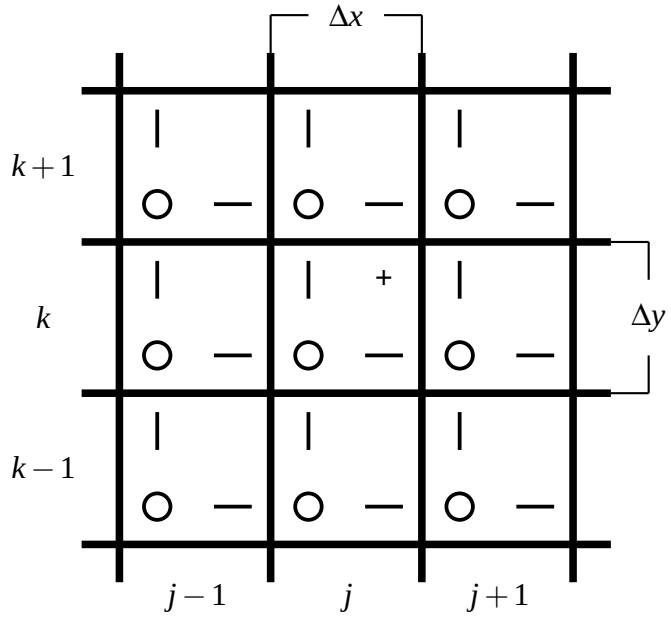

Figure 5: Displayed is the spatial grid and grid cells we use to solve (64) - (66) by numerical means. The grid increments are $\Delta x, \Delta y$, respectively in the x, y directions. There is a total of $J+1 \times K+1$ grid cells along the x- and y-axes, counted by using the dummy indices j,k. Circles, (O), correspond to h-, H- and η-points, horizontal dashes, $(-)$, to U-points, and vertical lines, $(|)$, to V-points. The point marked with a + is the position of the point x_j, y_k in grid cell j,k. The coordinates of the h-, H- and η-points in the grid are thus $x_j - \frac{1}{2}\Delta x$ and $y_k - \frac{1}{2}\Delta y$ as defined in (72). The coordinates of the U-points and V-points are as specified in (73)-(74), resepctively.

We also note that all terms appearing in (64) are evaluated at U-points, while all the terms appearing in (65) are evaluated at V-points. Likewise are all terms appearing in (66) evaluated at h-points.

3.1 Linear version

For the linear version we use a so called backward-forward scheme in time and a centered, second order scheme in space. This scheme was first suggested by *Sielecki* (1968) for rotating, linear shallow water equation. It corresponds to the scheme employed by *Martinsen et al.* (1979) in the first ever attempt to simulate storm surges in Norwegian waters numerically. Thus we get

$$\eta_{jk}^{n+1} = \eta_{jk}^{n} - \frac{\Delta t}{\Delta x} D_{jk}^{u} - \frac{\Delta t}{\Delta y} D_{jk}^{v}, \tag{75}$$

$$U_{jk}^{n+1} = U_{jk}^{n} + f\Delta t \overline{V}_{jk}^{n} + \frac{\Delta t}{\Delta x} P_{jk}^{u} + \frac{\Delta t}{\rho_0} \left[X_{jk}^{n+1} \right]^{u}, \tag{76}$$

$$V_{jk}^{n+1} = V_{jk}^{n} - f\Delta t \overline{U}_{jk}^{n+1} + \frac{\Delta t}{\Delta y} P_{jk}^{v} + \frac{\Delta t}{\rho_0} \left[Y_{jk}^{n+1} \right]^{v}, \tag{77}$$

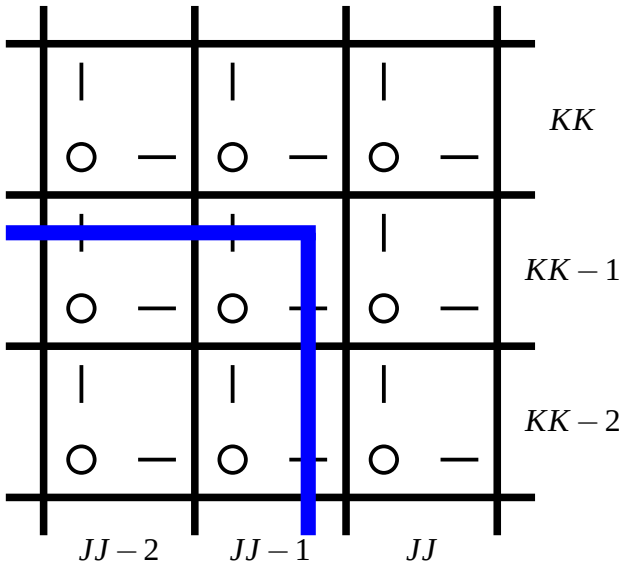

Figure 6: Displayed are the cells necessary to account for the no-slip boundary conditions at closed walls. In the sample shown we consider a case with solid walls in the upper right-hand corner of the grid. The walls are drawn as heavy solid blue lines. The notation is as in Figure 5, and the nine cells are thus numbered accordingly. Note that the cells (JJ,$KK-2$), (JJ,$KK-1$), (JJ,KK), ($JJ-1$,KK) and ($JJ-2$,KK) are outside of the land-sea boundary. As explained in the text their presence is, however, necessary to account for the no-slip boundary condition of no velocity at the walls.

where

$$D^u_{jk} = \left(U^n_{jk} - U^n_{j-1k}\right), \tag{78}$$

$$D^v_{jk} = \left(V^n_{jk} - V^n_{jk-1}\right), \tag{79}$$

are the divergence terms,

$$P^u_{jk} = -gH^u_{jk}\left(\eta^{n+1}_{j+1k} - \eta^{n+1}_{jk}\right) - \frac{H^u_{jk}}{\rho_0}\left(p_{s\,j+1k}^{\,n+1} - p_{s\,jk}^{\,n+1}\right), \tag{80}$$

$$P^v_{jk} = -gH^v_{jk}\left(\eta^{n+1}_{jk+1} - \eta^{n+1}_{jk}\right) - \frac{H^u_{jk}}{\rho_0}\left(p_{s\,jk+1}^{\,n+1} - p_{s\,jk}^{\,n+1}\right), \tag{81}$$

are the pressure terms,

$$\overline{U}^n_{jk} = \frac{1}{4}\left(U^n_{jk} + U^n_{j-1k} + U^n_{j-1k+1} + U^n_{jk+1}\right) \tag{82}$$

$$\overline{V}^n_{jk} = \frac{1}{4}\left(V^n_{jk} + V^n_{j+1k} + V^n_{j+1k-1} + V^n_{jk-1}\right). \tag{83}$$

represent the effect of the Earth's rotation (the Coriolis terms), and

$$\left[X_{jk}^{n+1}\right]^u = \left[\hat{X}_{jk}^{n+1}\right]^u - \frac{R\rho_0}{H_{jk}^u}U_{jk}^{n+1}, \tag{84}$$

$$\left[Y_{jk}^{n+1}\right]^v = \left[\hat{Y}_{jk}^{n+1}\right]^v - \frac{R\rho_0}{H_{jk}^v}V_{jk}^{n+1}. \tag{85}$$

are the combined wind and bottom stresses, where the notation $\hat{X},\hat{Y}$ is used to denote the wind stress components. Note that we make us of the superscripts u,v to remind ourselves that the respective terms are to be evaluated at a U-point, respectively V-point. We emphasize that because of the staggering the evaluation of the Coriolis terms are somewhat cumbersome in the C-grid, necessitating the use of the averaging of the nearest four grid points. We further emphasize that at the points next to solid boundaries the Coriolis terms must be changed to satisfy the boundary condition of no throughflow through solid boundaries. Essentially this involves changing the factor from one quarter to one half. Moreover, we observe that the pressure terms in (76) and (77) are evaluated at the new time step $n+1$, and so is the Coriolis term in (77). Thus as soon as a variable is updated we use the updated value in the next equation. This accounts for the reference to the scheme as a forward-backward scheme.

Regarding the stress terms (84) and (85) we recall that they are composed of two components, namely the wind stress whose common parameterization is given in (21) and the bottom friction whose parameterization is given in (23). We recall that the X component must be evaluated at U-points, while the Y component must be evaluated at V-points. This is already accounted for in the bottom stress terms, while for the wind stress we recall that they are specified as functions of (x,y,t) and thus are specified at the (x_j,y_k)-points (Figure 5). Thus we get

$$\rho_0\left[\hat{X}_{jk}^{n+1}\right]^u = \tau_s^x(x_j,y_k-\frac{1}{2}\Delta y,t^{n+1}) = \frac{1}{2}\left([\tau_s^x]_{jk}^n+[\tau_s^x]_{jk-1}^n\right), \tag{86}$$

$$\rho_0\left[\hat{Y}_{jk}^{n+1}\right]^v = \tau_s^y(x_j-\frac{1}{2}\Delta x,y_k,t^{n+1}) = \frac{1}{2}\left([\tau_s^y]_{jk}^n+[\tau_s^y]_{j-1k}^n\right). \tag{87}$$

Similarly we note that the equilibrium depth is specified at at the same points as h and η. Thus

$$H_{jk}^u = H_x(x_j,y_k-\frac{1}{2}\Delta y,t^{n+1}) = \frac{1}{2}\left(H_{j+1k}+H_{jk}\right) \tag{88}$$

while

$$H_{jk}^v = H_y(x_j-\frac{1}{2}\Delta x,y_k,t^{n+1}) = \frac{1}{2}\left(H_{jk+1}+H_{jk}\right). \tag{89}$$

3.2 Non-linear version

Since the forward-backward scheme does not work for the non-linear version we replace it by the leapfrog or centered in time and centered in space (CTCS) scheme. Thus we get

$$h_{jk}^{n+1} = h_{jk}^{n-1} - \frac{2\Delta t}{\Delta x} D_{jk}^{u} - \frac{2\Delta t}{\Delta y} D_{jk}^{v}, \tag{90}$$

$$U_{jk}^{n+1} = U_{jk}^{n-1} + 2f\Delta t \overline{V}_{jk}^{n} + \frac{2\Delta t}{\Delta x} N_{jk}^{u} + \frac{2\Delta t}{\Delta x} P_{jk}^{u} + \frac{2\Delta t}{\rho_0} \left[X_{jk}^{n+1} \right]^{u} + 2A\Delta t E_{jk}^{u}, \tag{91}$$

$$V_{jk}^{n+1} = V_{jk}^{n-1} - 2f\Delta t \overline{U}_{jk}^{n} + \frac{2\Delta t}{\Delta y} N_{jk}^{v} + \frac{2\Delta t}{\Delta y} P_{jk}^{v} + \frac{2\Delta t}{\rho_0} \left[Y_{jk}^{n+1} \right]^{v} + 2A\Delta t E_{jk}^{v}. \tag{92}$$

Here $D_{jk}^{u,v}$ represent the divergence terms, $\overline{U}_{jk}^{n}, \overline{V}_{jk}^{n}$ the Coriolis terms, $N_{jk}^{u,v}$ the non-linear terms, $P_{jk}^{u,v}$ the pressure terms, and $E_{jk}^{u,v}$ the eddy viscosity terms.

We first observe that the divergence terms, the Coriolis terms and the stress terms are unchanged and thus given by (78), (79), (82), (83), (84) and (85), respectively. Regarding the pressure terms we now get,

$$P_{jk}^{u} = -\frac{g}{2}(h_{j+1k}^{n} + h_{jk}^{n}) \left[(h_{j+1k}^{n} - h_{jk}^{n}) + (H_{j+1k} - H_{jk}) - \frac{1}{g\rho_0}(p_s{}_{j+1k}^{n+1} - p_s{}_{jk}^{n+1}) \right], \tag{93}$$

$$P_{jk}^{v} = -\frac{g}{2}(h_{jk+1}^{n} + h_{jk}^{n}) \left[(h_{jk+1}^{n} - h_{jk}^{n}) + (H_{jk+1} - H_{jk}) - \frac{1}{g\rho_0}(p_s{}_{jk+1}^{n+1} - p_s{}_{jk}^{n+1}) \right]. \tag{94}$$

For the eddy viscosity terms we use the Dufort-Frankel scheme. Thus we get

$$E_{jk}^{u} = \hat{E}_{jk}^{u} - \frac{\Delta x^2 + \Delta y^2}{\Delta x^2 \Delta y^2} U_{jk}^{n+1}, \tag{95}$$

$$E_{jk}^{v} = \hat{E}_{jk}^{v} - \frac{\Delta x^2 + \Delta y^2}{\Delta x^2 \Delta y^2} V_{jk}^{n+1}. \tag{96}$$

where

$$\hat{E}_{jk}^{u} = \frac{1}{\Delta x^2} \left(U_{j+1k}^{n} - U_{jk}^{n-1} + U_{j-1k}^{n} \right) + \frac{1}{\Delta y^2} \left(U_{jk+1}^{n} - U_{jk}^{n-1} + U_{jk-1}^{n} \right), \tag{97}$$

$$\hat{E}_{jk}^{v} = \frac{1}{\Delta x^2} \left(V_{j+1k}^{n} - V_{jk}^{n-1} + V_{j-1k}^{n} \right) + \frac{1}{\Delta y^2} \left(V_{jk+1}^{n} - V_{jk}^{n-1} + V_{jk-1}^{n} \right). \tag{98}$$

Note that the Dufort-Frankel scheme requires us to replace the terms $2U_{jk}^{n}$ and $2V_{jk}^{n}$ that would normally appear in a CTCS approximation to the eddy viscosity terms by the sum of its neighbors in time, that is, $2U_{jk}^{n} \to U_{jk}^{n+1} + U_{jk}^{n-1}$ and $2V_{jk}^{n} \to V_{jk}^{n+1} + V_{jk}^{n-1}$. The result is that the last terms on the right-hand side of (95) and (96) have to be moved to the left hand side of (91) and (92), respectively. This avoids using an elliptic solver, that is, (90) - (92) can still be solved explicitly as outlined in Section 4.

Finally we turn our attention to the non-linear terms included in (91) and (92). It turns out to be convenient to first define an average expressions for h similar to what we did for the volume transports in regarding the Coriolis terms, that is, (82) and (83). Thus we define

$$\overline{h}_{jk}^{n} = \frac{1}{4} \left(h_{jk}^{n} + h_{jk+1}^{n} + h_{j+1k+1}^{n} + h_{j+1k}^{n} \right). \tag{99}$$

By use of (99) we then get

$$N_{jk}^{u} = \frac{1}{4}\left\{ \frac{\left(U_{j+1k}^{n}+U_{jk}^{n}\right)^{2}}{h_{j+1k}^{n}} - \frac{\left(U_{jk}^{n}+U_{j-1k}^{n}\right)^{2}}{h_{jk}^{n}} , \right.$$
$$\left. + \frac{\Delta x}{\Delta y}\left[\frac{(U_{jk+1}^{n}+U_{jk}^{n})(V_{j+1k}^{n}+V_{jk}^{n})}{\overline{h}_{jk}^{n}} - \frac{(U_{jk}^{n}+U_{jk-1}^{n})(V_{j+1k-1}^{n}+V_{jk-1}^{n})}{\overline{h}_{jk-1}^{n}} \right] \right\}, \quad (100)$$

and

$$N_{jk}^{v} = \frac{1}{4}\left\{ \frac{\left(V_{jk+1}^{n}+V_{jk}^{n}\right)^{2}}{h_{jk+1}^{n}} - \frac{\left(V_{jk}^{n}+V_{jk-1}^{n}\right)^{2}}{h_{jk}^{n}} \right.$$
$$\left. + \frac{\Delta y}{\Delta x}\left[\frac{(U_{jk+1}^{n}+U_{jk}^{n})(V_{j+1k}^{n}+V_{jk}^{n})}{\overline{h}_{jk}^{n}} - \frac{(U_{j-1k+1}^{n}+U_{j-1k}^{n})(V_{jk}^{n}+V_{j-1k}^{n})}{\overline{h}_{jk-1}^{n}} \right] \right\}. \quad (101)$$

The application of Dufort-Frankel scheme regarding the eddy viscosity terms implies that the scheme is inconsistent. However, the eddy viscosity terms are added chiefly to keep the scheme from blowing up due to non-linear numerical instability. Thus the eddy viscosity does not represent any specific physics, but are added to prevent energy to accumulate at the shorter wavelengths. The eddy viscosity coefficient A therefore depends on the grid size and must be tuned so as to extract exactly the right amount of energy needed to mimic the energy loss to the sub-grid scale (SGS) motion.

4 Summary of the finite difference equations

We are now in a position to summarize and write down the finite difference equations (FDEs) that replace the linear and non-linear version of the continuous equations, that is, (69) - (71) for the linear version and (64) - (66) for the non-linear version. To make the presentation self sufficient we have reiterated all the terms present in the FDEs instead of referring back to their earlier definitions.

4.1 Linear version

For the linear version the FDE is just slightly different from those appearing in (75) - (77), that is,

$$\eta_{jk}^{n+1} = \eta_{jk}^{n} - \frac{\Delta t}{\Delta x}\left(U_{jk}^{n}-U_{j-1k}^{n}\right) - \frac{\Delta t}{\Delta y}\left(V_{jk}^{n}-V_{jk-1}^{n}\right), \quad (102)$$

$$U_{jk}^{n+1} = B_{jk}^{u}\left\{ U_{jk}^{n} + f\Delta t\overline{V}_{jk}^{n} + \frac{\Delta t}{\Delta x}P_{jk}^{u} + \frac{\Delta t}{\rho_0}\left[\hat{X}_{jk}^{n+1}\right]^{u} \right\}, \quad (103)$$

$$V_{jk}^{n+1} = B_{jk}^{v}\left\{ V_{jk}^{n} - f\Delta t\overline{U}_{jk}^{n+1} + \frac{\Delta t}{\Delta y}P_{jk}^{v} + \frac{\Delta t}{\rho_0}\left[\hat{Y}_{jk}^{n+1}\right]^{v} \right\}, \quad (104)$$

where

$$D^u_{jk} = \left(U^n_{jk} - U^n_{j-1k}\right), \quad D^v_{jk} = \left(V^n_{jk} - V^n_{jk-1}\right), \tag{105}$$

$$B^u_{jk} = \left(1 + \frac{R\Delta t}{H^u_{jk}}\right)^{-1}, \quad B^v_{jk} = \left(1 + \frac{R\Delta t}{H^v_{jk}}\right)^{-1}, \tag{106}$$

$$H^u_{jk} = \frac{1}{2}(H_{j+1k} + H_{jk}), \quad H^v_{jk} = \frac{1}{2}(H_{jk+1} + H_{jk}), \tag{107}$$

$$\overline{U}^n_{jk} = \frac{1}{4}(U^n_{jk} + U^n_{j-1k} + U^n_{j-1k+1} + U^n_{jk+1}), \tag{108}$$

$$\overline{V}^n_{jk} = \frac{1}{4}(V^n_{jk} + V^n_{j+1k} + V^n_{j+1k-1} + V^n_{jk-1}), \tag{109}$$

$$P^u_{jk} = -gH^u_{jk}\left(\eta^{n+1}_{j+1k} - \eta^{n+1}_{jk}\right) - \frac{H^u_{jk}}{\rho_0}\left({p_s}^{n+1}_{j+1k} - {p_s}^{n+1}_{jk}\right), \tag{110}$$

$$P^v_{jk} = -gH^v_{jk}\left(\eta^{n+1}_{jk+1} - \eta^{n+1}_{jk}\right) - \frac{H^v_{jk}}{\rho_0}\left({p_s}^{n+1}_{jk+1} - {p_s}^{n+1}_{jk}\right), \tag{111}$$

$$\left[\hat{X}^{n+1}_{jk}\right]^u = \frac{1}{2\rho_0}\left([\tau^x_s]^n_{jk} + [\tau^x_s]^n_{jk-1}\right), \tag{112}$$

$$\left[\hat{Y}^{n+1}_{jk}\right]^v = \frac{1}{2\rho_0}\left([\tau^y_s]^n_{jk} + [\tau^y_s]^n_{j-1k}\right). \tag{113}$$

respectively. The appearance of the factors $B^{u,v}_{jk}$ are due to our choice of evaluating the bottom stress at the new time level $n+1$, as specified in (84) and (85).

4.2 Non-linear version

The non-linear version is slightly more complicated because of the additional non-linear and eddy viscosity terms. Because we made use of the Dufort-Frankel scheme for the eddy viscosity terms an additional terms must be moved to the left-hand side, and hence the factors $B^{u,v}_{jk}$ must be expanded. Again it is only the momentum equations that are affected. Thus we get

$$h^{n+1}_{jk} = h^{n-1}_{jk} - \frac{2\Delta t}{\Delta x}D^u_{jk} - \frac{2\Delta t}{\Delta y}D^v_{jk}, \tag{114}$$

$$U^{n+1}_{jk} = B^u_{jk}\left\{U^{n-1}_{jk} + 2\Delta t\left(f\overline{V}^n_{jk} + \frac{1}{\Delta x}N^u_{jk} + \frac{1}{\Delta x}P^u_{jk} + \frac{1}{\rho_0}\left[\hat{X}^{n+1}_{jk}\right]^u + A\hat{E}^u_{jk}\right)\right\}, \tag{115}$$

$$V^{n+1}_{jk} = B^v_{jk}\left\{V^{n-1}_{jk} + 2\Delta t\left(-f\Delta t\overline{U}^n_{jk} + \frac{1}{\Delta y}N^v_{jk} + \frac{1}{\Delta y}P^v_{jk} + \frac{1}{\rho_0}\left[\hat{Y}^{n+1}_{jk}\right]^v + \hat{E}^v_{jk}\right)\right\}, \tag{116}$$

where

$$D^u_{jk} = \left(U^n_{jk} - U^n_{j-1k}\right), \quad D^v_{jk} = \left(V^n_{jk} - V^n_{jk-1}\right), \tag{117}$$

$$B^u_{jk} = \left[1 + \frac{R\Delta t}{H^u_{jk}} + \frac{2A\Delta t(\Delta x^2 + \Delta y^2)}{\Delta x^2 \Delta y^2}\right]^{-1}, B^v_{jk} = \left[1 + \frac{R\Delta t}{H^v_{jk}} + \frac{2A\Delta t(\Delta x^2 + \Delta y^2)}{\Delta x^2 \Delta y^2}\right]^{-1} \tag{118}$$

$$\overline{U}^n_{jk} = \frac{1}{4}(U^n_{jk} + U^n_{j-1k} + U^n_{j-1k+1} + U^n_{jk+1}), \tag{119}$$

$$\overline{V}^n_{jk} = \frac{1}{4}(V^n_{jk} + V^n_{j+1k} + V^n_{j+1k-1} + V^n_{jk-1}), \tag{120}$$

$$N^u_{jk} = \frac{1}{4}\left\{\frac{\left(U^n_{j+1k} + U^n_{jk}\right)^2}{h^n_{j+1k}} - \frac{\left(U^n_{jk} + U^n_{j-1k}\right)^2}{h^n_{jk}} + \frac{\Delta x}{\Delta y}\left[\frac{(U^n_{jk+1} + U^n_{jk})(V^n_{j+1k} + V^n_{jk})}{\overline{h}^n_{jk}} - \frac{(U^n_{jk} + U^n_{jk-1})(V^n_{j+1k-1} + V^n_{jk-1})}{\overline{h}^n_{jk-1}}\right]\right\}, \tag{121}$$

$$N^v_{jk} = \frac{1}{4}\left\{\frac{\left(V^n_{jk+1} + V^n_{jk}\right)^2}{h^n_{jk+1}} - \frac{\left(V^n_{jk} + V^n_{jk-1}\right)^2}{h^n_{jk}} + \frac{\Delta y}{\Delta x}\left[\frac{(U^n_{jk+1} + U^n_{jk})(V^n_{j+1k} + V^n_{jk})}{\overline{h}^n_{jk}} - \frac{(U^n_{j-1k+1} + U^n_{j-1k})(V^n_{jk} + V^n_{j-1k})}{\overline{h}^n_{jk-1}}\right]\right\}, \tag{122}$$

$$P^u_{jk} = \frac{g\Delta t}{\Delta x}\left[(h^n_{j+1k})^2 - (h^n_{jk})^2 - 2(h^n_{j+1k} + h^n_{jk})(H_{j+1k} - H_{jk})\right], \tag{123}$$

$$P^v_{jk} = \frac{g\Delta t}{\Delta y}\left[(h^n_{jk+1})^2 - (h^n_{jk})^2 - 2(h^n_{jk+1} + h^n_{jk})(H_{jk+1} - H_{jk})\right], \tag{124}$$

and finally

$$\left[\hat{X}^{n+1}_{jk}\right]^u = \frac{1}{2\rho_0}\left([\tau^x_s]^n_{jk} + [\tau^x_s]^n_{jk-1}\right), \tag{125}$$

$$\left[\hat{Y}^{n+1}_{jk}\right]^v = \frac{1}{2\rho_0}\left([\tau^y_s]^n_{jk} + [\tau^y_s]^n_{j-1k}\right), \tag{126}$$

$$\hat{E}^u_{jk} = \frac{1}{\Delta x^2}\left(U^n_{j+1k} - U^{n-1}_{jk} + U^n_{j-1k}\right) + \frac{1}{\Delta y^2}\left(U^n_{jk+1} - U^{n-1}_{jk} + U^n_{jk-1}\right), \tag{127}$$

$$\hat{E}^v_{jk} = \frac{1}{\Delta x^2}\left(V^n_{j+1k} - V^{n-1}_{jk} + V^n_{j-1k}\right) + \frac{1}{\Delta y^2}\left(V^n_{jk+1} - V^{n-1}_{jk} + V^n_{jk-1}\right). \tag{128}$$

4.3 Numerical stability condition

We note that the above schemes are numerically stable provided the Courant-Friedrich-Levy (CFL) condition is satisfied. If we let $\Delta x = \Delta y = 2\Delta s$ and $c_0 = \sqrt{gH_{max}}$, where H_{max} denotes

the maximum equilibrium depth, the CFL condition reads

$$\Delta t \leq \frac{\Delta s\sqrt{2}}{c_0}, \tag{129}$$

provided $\Delta s << L_R$, where $L_R = c_0/f$ is the Rossby radius of deformation.

4.4 Implementation of boundary conditions

We emphasize that the above FDEs are valid only away from any physical boundaries. As for the continuous equations the boundary conditions prevail at the boundaries of the domain. As alluded to this has some numerical consequences regarding the Coriolis terms, the non-linear terms and the eddy viscosity terms. in order to properly satisfy the boundary conditions in our FDEs. We underscore that the one of the main reason for using a staggered grid is to avoid over-specifying the number of boundary conditions. The number of specified boundary condition should exactly match the number of integration constants of the continuous, governing equations (e.g., *Røed*, 2011).

4.4.1 Closed boundaries

Let us first consider a motion within a rectangular domain bounded by solid, impermeable walls on the four sides. Accordingly we have to change the FDEs for the points next to any boundary to account for this fact. As alluded to in Section 3 it is common, if we employ the staggered C-grid, to let the boundaries go through U-points and V-points as displayed in Figure 6. Thus the physical condition of no flow through an impermeable wall is satisfied by letting $U = 0$ and $V = 0$ along the respective boundaries in the appropriate cells.

In particular we have to reevaluate the Coriolis term in the cells neighboring a solid boundary to avoid spurious residual flows close to the boundary using the "wet-point-only" method first suggested by (*Jamart and Ozer*, 1986). Looking at Figure 6, featuring a solid boundary through the V-points in the cells numbered $(j, KK-1)$, we notice that the averaging of the Coriolis term in (104), that is, $\overline{V}^{n+1}_{jk}$ consists of four terms of which two of them are zero. Hence the factor must be changed to one half instead of one fourth, that is, at these points $\overline{V}^{n}_{jk}$ in (109) and (120) is replaced by

$$\overline{V}^{n}_{jKK-1} = \frac{1}{2}(V^{n}_{j,KK-2} + V^{n}_{jKK-2}). \tag{130}$$

Similarly follows that if there are solid walls along all boundaries that

$$\overline{V}^{n}_{j2} = \frac{1}{2}(V^{n}_{j2} + V^{n}_{j+12}), \tag{131}$$

$$\overline{U}^{n+1}_{2k} = \frac{1}{2}(U^{n+1}_{2k+1} + U^{n+1}_{2k}), \tag{132}$$

$$\overline{U}^{n+1}_{JJ-1k} = \frac{1}{2}(U^{n+1}_{JJ-2k+1} + U^{n+1}_{JJ-2k}). \tag{133}$$

For the non-linear version the number of integration constants are increased due to the appearance of the eddy viscosity terms. Thus we also require the velocity along closed, solid walls to be zero as well, that is, both $U = 0$ and $V = 0$ must be satisfied at all boundaries. We note that there are no U-points along the boundaries through V-points, and vice versa. One way to satisfy the boundary condition of no flow tangentially along the (physical) boundary is to interpolate across the boundary, so that the interpolated value at the boundary becomes zero. As displayed in Figure 6 we achieve this by adding the cells outside of the boundary, and let the value of the transport component in question be "mirrored". For instance look at the U-points along the $k = KK - 1$ closed boundary in Figure 6. To satisfy the condition of $U = 0$ at the boundary we simply let $U^n_{jKK} = -U^n_{jKK-1}$ for all j (linear interpolation). Similarly we let $V^n_{JJk} = -V^n_{JJk}$ for $j = JJ$ for all k.

4.4.2 Open boundaries

At open boundaries the governing equations are still valid. However, since our grid is finite we have to specify a boundary condition within the cells featuring open boundaries. A host of such conditions exist in the literature (e.g., *Røed and Cooper*, 1987; *Palma and Matano*, 2000). A common denominator is that none of them are perfect.

We employ a particular simple one based on the so called Flow Relaxation Scheme (FRS) suggested by *Martinsen and Engedahl* (1987), but first suggested for use in numerical weather prediction (e.g., *Davies*, 1976). The variables in the open boundary cell is first calculated simply by using a one-dimensional version of the governing equations. Commonly this solution is referred to as the external solution to separate it from the internal solution, that is, the solution of the true governing equation. Next we relax the internal solution to the external solution through a buffer zone.

For instance, let the internal solution at time level $n+1$ before relaxation be ψ^*_{jk} in all cells except for the boundary cells, where ψ is any of the prognostic variables. Furthermore, let the external solution at time level $n+1$ be ψ^{en+1}_{jk}. We obtain the solution at the new time step $n+1$ for the entire domain including the boundary cells by performing a simple relaxation, that is,

$$\psi^{n+1}_{jk} = (1-\alpha_{jk})\psi^*_{jk} + \alpha_{jk}\psi^{en+1}_{jk}, \tag{134}$$

where α_{jk} is a number between zero and one such that it varies monotonically from $\alpha_{jk} = 0$ inside of the buffer zones, that is, in the domain of interest, to $\alpha_{jk} = 1$ in the boundary cells. Thus within the domain of interest $\psi^{n+1}_{jk} = \psi^*_{jk}$, while in the boundary cells $\psi^{n+1}_{jk} = \psi^{en+1}_{jk}$.

As an example let us consider that the upper boundary displayed in Figure 6. The cells j, KK for all j are then open boundary cells. The external solution is found by use of the governing (69) - (71) by neglecting all terms with a derivative across the boundary. In this implies $\partial_y = 0$. Thus we get

$$\partial_t \eta^e = -\partial_x U, \tag{135}$$
$$\partial_t U^e = fV^e - gH\partial_x \eta^e + X, \tag{136}$$
$$\partial_t V^e = -fU^e + Y, \tag{137}$$

where we have dropped the sea surface pressure term. Similarly the FDEs to compute the external solutions may be derived from (102) - (104). If we assume the computational domain to be rectangular with open boundaries along the *y*-axis to the left and right, then we get

$$\eta^{en+1}_k = \eta^{en}_k - \frac{\Delta t}{\Delta x} D^u_k, \tag{138}$$

$$U^{en+1}_k = B^u_k \left\{ U^{en}_k + f\Delta t \overline{V^e}^n_k - gH^u_k \frac{\Delta t}{\Delta x}(\eta^{en}_{k+1} - \eta^{en}_k) + \Delta t \left[\hat{X}^{n+1}_k\right]^u \right\}, \tag{139}$$

$$V^{en+1}_k = B^v_k \left\{ V^{en}_k - f\Delta t \overline{U^e}^{n+1}_k + \Delta t \left[\hat{Y}^{n+1}_k\right]^v \right\}, \tag{140}$$

where

$$D^u_k = U^{en}_k - U^{en}_{k-1}, \quad B^u_k = \left(1 + \frac{R\Delta t}{H^u_k}\right)^{-1}, \tag{141}$$

$$B^v_k = \left(1 + \frac{R\Delta t}{H^v_k}\right)^{-1}, \quad H^u_k = \frac{1}{2}(H_{k+1} + H_k), \tag{142}$$

$$\overline{U^e}^n_k = \frac{1}{2}(U^{en}_k + U^{en}_{k-1}), \quad \overline{V^e}^n_k = \frac{1}{2}(V^{en}_k + V^{en}_{k+1}), \tag{143}$$

$$\left[\hat{X}^{n+1}_k\right]^u = \frac{1}{2\rho_0}\left([\tau^x_s]^n_k + [\tau^x_s]^n_{k-1}\right), \tag{144}$$

$$\left[\hat{Y}^{n+1}_k\right]^v = \frac{1}{\rho_0}[\tau^y_s]^n_k, \tag{145}$$

5 Summary and final remarks

To summarize we have showed how simple one-layer, two-layer and $1\frac{1}{2}$-layer ocean models may be derived from the full Reynolds Average Navier-Stokes (RANS) equations, and how the one-layer model in particular may be replaced by finite difference equation. Both the linear version and the non-linear version were included.

The rationale behind this derivation is to pave the way for use of these simple models in ensemble prediction systems. Furthermore we would like to investigate the possibility of solving these equations numerically making use of the computers Graphical Processing Units (GPUs) rather than the Central Processing Units. To solve these equations on GPUs require computer programs different form the traditional FORTRAN program language and other common program languages in use today (e.g. C++). Thus solutions to well defined benchmark case, by which the solutions using GPUs may be verified, are needed. In the accompanying Part II (*Røed*, 2012) we therefore present such solutions. The benchmark cases are solved using the traditional FORTRAN program language and Part II also present the FORTRAN source code used to generate the solutions.

References

Busallacchi, A. J., and J. J. O'Brien (1980), The seasonal variability in a model of the tropical Pacific, *J. Phys. Oceanogr.*, *10*, 1929–1951.

Busallacchi, A. J., and J. J. O'Brien (1981), Interannual variability of the equatorial pacific in the 1960's, *J. Geophys. Res.*, *86*, 10,901–10,907.

Charney, J. G., and M. E. Stern (1962), On the stability of internal baroclinic jets in a rotating atmosphere, *J. Atmos. Sci.*, *19*, 159–172.

Cushman-Roisin, B., and J. O'Brien (1983), The influence of bottom topography on baroclinic transports, *J. Phys. Oceanogr.*, *1600-1611*, 227–239.

Davies, H. C. (1976), A lateral boundary formulation for multilevel prediction models, *Quart. J. Roy. Meteor. Soc.*, *102*, 405–418.

Engedahl, H. (1995b), Implementation of the Princeton Ocean Model (POM/ECOM-3D) at the Norwegian Meteorological Institute (DNMI)., *Research Report 5*, Norwegian Meteorological Institute.

Gill, A. E. (1982), *Atmosphere-ocean dynamics*, *International Geophysical Ser.*, vol. 30, Academic Press.

Griffies, S. M. (2004), *Fundamentals of ocean climate models*, Princeton University Press.

Hackett, B., and L. P. Røed (1998), A numerical study of the slope current northwest of the British Isles, *Cont. Shelf Res.*, *18*, 1–30.

Haltiner, G. J., and R. T. Williams (1980), *Numerical prediction and dynamic meteorology, second edition*, 477 pp., John Wiley & Sons.

Heburn, G. W. (1988), A numerical study of the western Mediterranean Sea, *Rapport Commision pour l'Exploration Scientifique de la Mer Méditerranée*, *31*(2), 210.

Heburn, G. W., and P. E. LaViolette (1990), Variations in the structure of the anticyclonic gyres found in the Alboran Sea, *J. Geophys. Res.*, *95*(C2), 1599–1614.

Hurlburt, H. E., and J. D. J. Dana Thompson (1976), A numerical study of the Somali current, *J. Phys. Oceanogr.*, *6*, 646–664.

Hurlburt, H. E., and J. D. J. Dana Thompson (1980), A numerical study of loop current intrusions and eddy shedding, *J. Phys. Oceanogr.*, *10*(10), 1611–1651, doi:10.1175/1520-0485(1980)010¡1611:ANSOLC¿2.0.CO;2.

Hurlburt, H. E., J. C. Kindle, and J. J. O'Brien (1976), A numerical simulation of the onset of El Niño, *J. Phys. Oceanogr.*, *6*, 621–631.

Jamart, B. M., and J. Ozer (1986), Numerical boundary layers and spurious residual flows, *J. Geophys. Res.*, *91*, 10,621–10,631.

Kindle, J. C., and J. D. Thompson (1989), The 26- and 50- day oscillation in the western Indian Ocean: Model results, *J. Geophys. Res.*, *94*, 4721–4736.

Luther, M. E., and J. J. O'Brien (1985), A model of the seasonal circulation in the Arabian Sea forced by observed winds, *Progr. Oceanogr.*, *14*, 353–385.

Martinsen, E. A., and H. Engedahl (1987), Implementation and testing of a lateral boundary scheme as an open boundary condition in a barotropic ocean model., *Coast. Eng.*, *11*, 603–627.

Martinsen, E. A., B. Gjevik, and L. P. Røed (1979), A numerical model for long barotropic waves and storm surges along the western coast of norway, *J. Phys. Oceanogr.*, *9*, 1126–1138.

McCreary, J. P., and P. K. Kundu (1988), A numerical investigation of the Somali Current during the southwest monsoon, *J. Mar. Res.*, *46*, 25–58.

Mesinger, F., and A. Arakawa (1976), Numerical methods used in atmospheric models, GARP Publication Series No. 17, 64 p., World Meteorological Organization, Geneva, Switzerland.

Palma, E. D., and R. P. Matano (2000), On the implementation of open boundary conditions to a general circulation model: The 3-d case., *J. Geophys. Res.*, *105*, 8605–8627.

Phillips, N. A. (1957), A coordinate system having some special advantages for numerical forecasting, *J. Meteorology*, *14*, 184–185.

Potemra, J. T., M. E. Luther, and J. J. O'Brien (1991), The seasonal circulation of the upper ocean in the Bay of Bengal, *J. Geophys. Res.*, *96*, 12,667–12,683.

Preller, R. (1986), A numerical study of the Alboran Sea gyre, *Prog. Oceanogr.*, *16*, 113–146.

Røed, L. P. (1979), Storm surges in stratified seas, *Tellus*, *31*, 330–339.

Røed, L. P. (1995), Documentation of the Oslo Multilayer Mesoscale Ocean Model - OSMOM, Part 1: The governing equations, *Research Report 24*, Norwegian Meteorological Institute, [Available from Norwegian Meteorological Institute, Postboks 43 Blindern, N-0313 Oslo, Norway].

Røed, L. P. (1996), Modeling mesoscale features in the ocean, in *Waves and Nonlinear Processes in Hydrodynamics, Fluid Mechanics and its applications*, vol. 34, edited by J. Grue, B. Gjevik, and J. E. Weber, pp. 383–396, Kluwer Academic Publishers.

Røed, L. P. (1997), Energy diagnostics in a $1\frac{1}{2}$-layer, nonisopycnic model, *J. Phys. Oceanogr.*, *27*, 1472–1476.

Røed, L. P. (1999), A pointwise energy diagnostic scheme for multilayer, nonisopycnic, primitive equation ocean models, *Mon. Weath. Rev.*, *127*, 1897–1911.

Røed, L. P. (2011), Atmospheres and Ocean on Computers: Fundamentals, Lecture notes to GEF4510 fall 2011, Department of Geosciences, University of Oslo, P.O. Box 1022 Blindern, 0315 Oslo, Norway, 162 pp.

Røed, L. P. (2012), Documentation of simple ocean models for use in ensemble predictions. part II: Benchmarks, *met.no Report xx/2012*, Norwegian Meteorological Institute, Box 43 Blindern, N-0313 Oslo, Norway.

Røed, L. P., and C. K. Cooper (1987), A study of various open boundary conditions for wind-forced barotropic numerical ocean models, in *Three-dimensional models of marine and estuarine dynamics*, *Elsevier Oceanography Series*, vol. 45, edited by J. C. J. Nihoul and B. M. Jamart, pp. 305–3, Elsevier Science Publishers B.V.

Røed, L. P., and X. B. Shi (1999), A numerical study of the dynamics and energetics of cool filaments, jets and eddies off the Iberian Peninsula, *J. Geophys. Res.*, *104*, 29,817–29,841.

Shi, X. B., and L. P. Røed (1999), Frontal instability in a two-layer, primitive equation ocean model, *J. Phys. Oceanogr.*, *29*, 948–968.

Sielecki, A. (1968), An energy-conserving numerical scheme for the solution of the storm surge equations, *Mon. Weather Rev.*, *96*, 150–156.